crystals

MDPI

Article

Microstructure and Corrosion Behaviour of Mg-Ca and Mg-Zn-Ag Alloys for Biodegradable Hard Tissue Implants

Lavinia Dragomir (Nicolescu) [1], Iulian Antoniac [1,2,*], Veronica Manescu (Paltanea) [1,3], Aurora Antoniac [1], Marian Miculescu [1], Octavian Trante [1], Alexandru Streza [1], Cosmin Mihai Cotruț [1] and Doriana Agop Forna [4]

[1] Faculty of Material Science and Engineering, University Politehnica of Bucharest, 313 Splaiul Independentei St., 060042 Bucharest, Romania; laavinia.dragomir@gmail.com (L.D.); veronica.paltanea@upb.ro (V.M.); antoniac.aurora@gmail.com (A.A.); marian.miculescu@upb.ro (M.M.); octavian.trante@upb.ro (O.T.); alexandru_streza@yahoo.com (A.S.); cosmin.cotrut@upb.ro (C.M.C.)
[2] Academy of Romanian Scientists, 54 Splaiul Independentei St., 050094 Bucharest, Romania
[3] Faculty of Electrical Engineering, University Politehnica of Bucharest, 313 Splaiul Independentei St., 060042 Bucharest, Romania
[4] Faculty of Dental Medicine, Grigore T. Popa University of Medicine and Pharmacy, 16 Universitatii St., 700115 Iasi, Romania; drdorianaforna@gmail.com
* Correspondence: antoniac.iulian@gmail.com

Abstract: Trauma orthopaedic surgery was the first domain to use degradable metallic implants made of magnesium alloys since the early 20th century. Unfortunately, the major limitation that consists of rapid degradation and subsequent implant failure, which occur in physiological environments with a pH between 7.4 and 7.6, prevents its widespread application. The biggest challenge in corrosion assay is the choice of the testing medium in order to reproduce more closely in vivo conditions. The current study was focused on two Mg-Zn-Ag alloys (Mg7Zn1Ag and Mg6Zn3Ag) and the Mg1Ca alloy. Dulbecco's Modified Eagle Medium (DMEM) and Kokubo's simulated body fluid solution (SBF) were selected as testing mediums and we follow the corrosion evaluation by the corrosion rate and mass loss. Also, the corrosion behaviour was interpreted in correlation with the microstructural features and alloying elements of the experimental magnesium-based alloys revealed by optical microscopy (OM), X-ray diffraction (XRD), and scanning electron microscopy (SEM) coupled with energy dispersive spectroscopy (EDX). The experimental results highlight the more corrosive nature of the SBF environment and that a higher percentage of silver (2.5 wt.%) exhibited a better corrosion resistance. We consider that the magnesium alloy Mg6Zn3Ag showed valuable biodegradation characteristics to be considered as raw materials for manufacturing small trauma implants.

Keywords: magnesium alloys; corrosion rate; microstructure; implant

check for updates

Citation: Dragomir, L.; Antoniac, I.; Manescu, V.; Antoniac, A.; Miculescu, M.; Trante, O.; Streza, A.; Cotruț, C.M.; Forna, D.A. Microstructure and Corrosion Behaviour of Mg-Ca and Mg-Zn-Ag Alloys for Biodegradable Hard Tissue Implants. *Crystals* **2023**, *13*, 1213. https://doi.org/10.3390/cryst13081213

Academic Editors: Erdem Karakulak and Huseyin Sevik

Received: 14 July 2023
Revised: 2 August 2023
Accepted: 3 August 2023
Published: 5 August 2023

Copyright: © 2023 by the authors. Licensee MDPI, Basel, Switzerland. This article is an open access article distributed under the terms and conditions of the Creative Commons Attribution (CC BY) license (https://creativecommons.org/licenses/by/4.0/).

1. Introduction

Today, biodegradable alloys containing magnesium and exhibiting high osseointegration capacity are used in orthopaedic implant manufacture. Magnesium is characterized by mechanical properties much closer to that of the human bone than classic metallic biomaterials such as cobalt-chromium, titanium and its alloys, and stainless steel [1,2]. According to previous studies, temporary magnesium trauma implants exhibit excellent mechanical properties, good biodegradability, and biocompatibility [1,3,4].

Trauma orthopaedic surgery was the first domain to use degradable metallic implants made of magnesium alloys since the early 20th century [4]. Unfortunately, the major limitation that consists of rapid degradation and subsequent implant failure, which occurs in physiological environments with a pH between 7.4 and 7.6 [5], prevents its widespread application. Due to this process, alkaline ions will likely accumulate locally, leading to cytotoxicity and inflammation [6]. Another critical problem that can have a negative effect [6,7] is the production of hydrogen (H_2) gas during degradation [8]. These accumulated gas

bubbles have the potential to obstruct healthy blood flow, throw off the parameters of blood cells, harm nearby tissue, and even spread infection [9–11]. Another concerning issue with the use of magnesium alloys in medicine is the localized corrosion phenomenon that can happen due to galvanic cell formation, corrosive conditions, and high-strain regions, which contribute to mechanical integrity loss [12–14].

Moreover, magnesium is very reactive and forms a double layer of magnesium oxide (MgO) and magnesium hydroxide ($Mg(OH)_2$) on its surface in an aqueous environment. This layer does not offer enough corrosion protection through the passivation mechanism. As a direct consequence, the magnesium degrades at a rate that makes it inappropriate for long-term implant use. On the other hand, it can be considered one of the best materials for temporary implant manufacture [15].

In order to eliminate these drawbacks, different solutions were proposed, such as implant surface coating based on methods, which permit the material microstructure change and improve the surface quality while reducing roughness, alloying of the Mg-based materials with other metals, and new compounds or additives' use. According to several studies, an increase in the corrosion resistance of magnesium-based materials could be obtained by the addition of some alloying elements like calcium (Ca), zinc (Zn), manganese (Mn), and rare earth (RE). Also, surface modification is considered an adequate method for enhancing the functionality of magnesium-based alloys in the orthopaedic application field [16].

Magnesium-based alloys have once again been the subject of research for scientists such as Witte, Xu, and Staiger [4,17,18]. Mg-Al-Zn, denoted by the abbreviation AZ, was one of the most investigated materials in the literature. The experiments revealed a direct connection between degradation speed in different media and the percentage of alloying elements. In this direction, through RE addition, the corrosion rate of the Mg-based alloys was reduced by a high amount [19]. Also, different thermal and thermo-mechanical treatments can be applied to control the material corrosion rate. It was noticed that based on these methods, a refined grain structure, characterized by a controlled secondary phase distribution, was obtained.

Many in vitro and in vivo tests are performed to understand and analyse the local corrosion mechanisms that occur between modified implant surfaces and local environments [19]. It is well known that the corrosion mechanisms inside the human body are much more complex than in fluids containing only water. This process is influenced by the solution pH, ion nature and concentration, biochemical activity of the human tissues placed near the implant, and protein adsorption process [20,21]. The degradation products can be beneficial against the corrosion process through the apparition of a protective layer. It was shown that higher corrosion rates were determined during in vitro experiments compared to in vivo studies [20]. The degradation rate of the implant should be equal to the bone tissue healing rate in an ideal situation [22]. By considering this, Steiger et al. [18] established that implant replacement with healthy bone occurred 12 weeks after the trauma treatment was initiated.

The electrochemical analysis is considered simple and reproducible, but it accelerates the corrosion process, which is not necessarily related to in vivo degradation. For example, Zhang et al. [13] reported a degradation rate of 0.26 mm/year determined through the immersion method and 2.52 mm/year in the case of the electrochemical method for pure magnesium. The biggest challenge in corrosion assay is the choice of the test environment because it is imperative to use solutions that reproduce in vivo conditions. The most appropriate test media are Simulated Body Fluid (SBF), Dulbecco's Modified Eagle's Medium (DMEM), Hank's balanced salt solution (HBSS), Kirkland's biocorrosion medium (KBM), Earle's balanced salt solution (EBSS), Minimum Essential Medium (MEM), and Eagle's Minimum Essential Medium (E-MEM) [23]. The Hank's, EBSS, KBM, DMEM, E-MEM, and MEM present Dex/glucose since amino acids are included in DMEM, E-MEM, and MEM. Further, DMEM also contains vitamins. Similar chemical compositions to human

plasma were noticed in the case of SBF and Hank's solutions, so they are widely used to analyse the corrosion rate of Mg-based alloys for biomedical applications.

The buffering system used in simulated body fluid is useful because it can accelerate the degradation rate of Mg-based alloys. Usually, the following buffers are involved: tris-hydroxymethyl aminomethane (Tris-HCl), CO_2/$NaHCO_3$, and 4-(2-hydroxyethyl)-1-piperazineethanesulfonic acid (HEPES) [23]. It was shown that HEPES reduces the calcium phosphate and carbonate formation in the corrosion layer [24,25]. On the other side, Tris-HCl accelerates the degradation of pure Mg due to the consumption effect of OH^- ions [26]. Other factors which have a strong influence on the corrosion rate of Mg-based alloys are the pressure and concentration of CO_2 [27], the SO_4^{2-} concentration that plays an important role in the Mg corrosion rate increase [26], and the number and quantity of organic components, which control the solution pH [27]. Some of the most important studies of immersion tests made under physiological conditions [28–33] to study the Mg-based alloys degradation rate are presented in Table 1.

Table 1. Research conducted under physiological conditions to investigate the Mg-based corrosion characteristics [28–33].

Mg-Based Alloy	Simulated Physiological Solution for Corrosion Studies	Medium Used for Cell Culture	Conditions	Biological Tests	Reference
Pure Mg	1 M NaOH for 24 h or M-SBF for 5 days	EMEM	Cell culture *, immersion time-24 h	Human HeLa cells, GSP-C12 mouse fibroblasts	[28]
Mg-4Y-3RE-0.5Zr (WE43)	SBF	HBSS	Cell culture *, immersion time-72 h	Human umbilical vein endothelial cells	[29]
Pure Mg, Mg-Ca, Mg-Mn, Mg-Zn	-	MEM + 10% FBS	Cell culture *, immersion time-24, 48, 96 h	L929 cells SaOS-2 cells	[30]
Mg-Zn-Ca, AZ31 (Mg-3Al-1Zn)	DMEM	DMEM + 10% FBS + 1 P (Penicillin)/S (streptomycin)	Cell culture *, immersion time-168 h	Unspecified cellular line	[31]
Pure Mg, Mg-4Y-3RE, Mg-5Gd, Mg-10Gd, Mg-2Ag, Mg-4Ag, Mg-6Ag	DMEM Glutamax	-	Cell culture *, immersion time-200 h	Absence of biological tests	[32]
Pure Mg	DMEM	DMEM	Cell culture *, immersion time: 384 h	In vitro–vivo test consisting of sample implantation in the murine artery	[33]

* Cell culture = cell culture conditions (37 °C, 5% CO_2, 95% rH).

Factors including porosity, grain size, composition, and secondary phase presence also influence the corrosion of Mg-based alloys. More specifically, grain size plays a crucial role in mechanical properties values such as elastic limit and hardness as well as how corrosion of metals affects them. The most common alloying elements for Mg are Zinc (Zn), Calcium (Ca), Lithium (Li), Manganese (Mn), Zirconium (Zr), Aluminium (Al), Silver (Ag), Strontium (Sr), and Yttrium (Y). Table 2 summarizes how these alloying elements affect magnesium degradation behaviour [34–43].

The analysis of magnesium degradation has made significant progress over the last decade, leading to models that predict the rate of in vivo degradation. However, the mechanisms still need to be fully understood, and more effort is needed to determine them.

Table 2. Influence of alloying elements on the degradation behaviour of Mg-based alloys.

Alloying Elements	Effect of Degradation Behaviour	Ref.
Ca	Less than 1 wt.% Ca should be present in magnesium alloys; a higher Ca addition has a negative influence on corrosion resistance.	[36,37]
Mn	With less than 1 wt.% Mn, the corrosion resistance is increased by reducing impurities.	[38]
Zn	Increasing the corrosion resistance of magnesium alloys, primarily at a content below 5 wt.%.	[39]
Zr	Zr content under 2 wt.% percent raising corrosion resistance.	[40]
Li	Increasing corrosion resistance at concentrations lower than 9 wt.% in pure Mg; higher Li additions decrease corrosion resistance.	[41]
Sr	Corrosion resistance is affected; a content level under 2 wt.% is ideal.	[42]
Al	By increasing Al content (the maximum is reached at a solubility limit of 12.7 wt.% Al) a decrease in the corrosion rate of the homogenous α-phase was noticed.	[43]
RE	General improvement in the corrosion resistance of Mg alloys. The corrosion resistance of Mg-light REE alloys was generally better than that of Mg-heavy REE alloys	[35]

The beneficial grain-refining effect in Mg-Ca alloys occurs at a calcium content of up to 1 wt.%. Although from an electrochemical point of view, the intermetallic compound from its structure is more active than pure magnesium, in vitro and in vivo studies have shown that small additions of Ca (less than 1%) increase the corrosion resistance of the alloy since no grain growth was observed, and leads to the reduction of their size in the microstructure of the casting Mg-Ca alloys [4,19,44,45].

Due to their ability to prevent and treat implant-related infections, biodegradable Mg-Ag alloys represent an important class of materials potentially used for orthopaedic implants [46,47]. The corrosion behaviour of Mg-based alloys is strongly influenced by the Ag content due to the fact that the addition of Ag decreases the grain size and increases the standard electrode potential. But a large amount of Ag in these alloys can have the opposite effect by accelerating micro-galvanic corrosion between the Mg matrix and Ag-rich precipitates.

Considering these aspects, the current study was focused on two alloys from the Mg-Zn-Ag system, respectively, Mg7Zn1Ag and Mg6Zn3Ag, and the Mg1Ca alloy. The in vitro research performed aims to evaluate the influence of the microstructure and the used test media on the corrosion behaviour of the above-mentioned Mg-based alloys. The mass loss and corrosion rate were used to highlight the corrosion behaviour. Also, the corrosion behaviour was interpreted in correlation with the microstructural features and alloying elements of the experimental magnesium-based alloys revealed by optical microscopy (OM) scanning electron microscopy (SEM) coupled with energy dispersive spectroscopy (EDX), and X-ray diffraction (XRD).

2. Materials and Methods

In the present paper, two Mg-based alloys from the Mg-Zn-Ag ternary system and one of the Mg-Ca system, with the chemical composition presented in Table 3, were investigated. Alloys were obtained by the melt-casting method described previously [48–50].

Table 3. Chemical composition of the investigated Mg-based alloys.

Alloys	Composition (wt.%)			
	Zn	**Ag**	**Ca**	**Mg**
Mg7Zn1Ag	7.2	1.5	-	Bal.
Mg6Zn3Ag	6.4	2.5	-	Bal.
Mg1Ca	-	-	1	Bal.

Cuboidal samples with dimensions of 15 × 15 × 5 mm were cut for materials characterization (microstructure and phase composition) and in vitro corrosion study. Prior to the investigations, the samples were mechanically polished using silicon carbide paper (600–2000 grit), polished, and ultrasonically cleaned in ethanol.

2.1. Materials Characterization

The magnesium-based alloys microstructure was highlighted by scanning electron microscopy and optical microscopy using an FEI QUANTA INSPECT F microscope (FEI Company, Eindhoven, Netherlands) with an energy dispersive spectroscopy and an Olympus BX51 microscope (Olympus Life and Materials Science Europa GMBH, Hamburg, Germany).

The phase identification from the structure of the Mg-based alloy samples was highlighted by X-ray Diffraction (XRD) (Malvern Panalytical Ltd., Malvern, Great Britain) and the PDXL Software Version 1.2.0.1 (ICDD 1999). The equipment involved in this analysis was a Panalytical X-Pert PRO diffractometer with CuKα radiation.

2.2. In Vitro Corrosion Study

The corrosion behaviour of the investigated Mg-based alloys was assessed through immersion and electrochemical corrosion tests. The tests were performed using two testing media: Kokubo's simulated body fluid solution (SBF, prepared in our laboratory according to [51]) and Dulbecco's Modified Eagle Medium (DMEM, Merck KGaA, Darmstadt, Germany), whose compositions are given in Table 4. As a pH buffer in Kokubo's simulated body fluid solution, we used tris-hydroxymethyl aminomethane (TRIS-HCl), while the DMEM solution contains [4-(2-hydroxyethyl)-1-piperazineethanesulfonic acid] (HEPES).

Table 4. The composition of the SBF and DMEM testing media.

Medium	SBF (ISO 23317:2014)	DMEM
	Ion concentration (mM)	
Na^+	142	156
K^+	5	5.33
Mg^{2+}	1.5	0.81
Ca^{2+}	2.5	1.8
Cl^-	147.8	121
HCO_3^-	4.2	0.91
HPO_4^{2-}	1.0	44.1
SO_4^{2-}	0.5	0.81
	Organic components (mM)	

Table 4. *Cont.*

Medium	SBF (ISO 23317:2014)	DMEM
Amino acids: Glycine, L-Cystine 2HCl, L-Glutamine, L-Isoleucine, L-Leucine, L-Lysine hydrochloride, L-Methionine, L-Phenylalanine, L-Serine, L-Threonine, L-Tryptophan, L-Valine, L-Arginine hydrochloride, L-Tyrosine disodium salt dihydrate, L-Histidine hydrochloride-H_2O	-	10.6801
Vitamins: Choline chloride, D-Calcium pantothenate, Folic acid, Niacinamide, Pyridoxine hydrochloride, Riboflavin, Thiamine hydrochloride, i-Inositol	-	0.1515
Other: D-Glucose, Sodium Pyruvate, Phenol red	-	5.5399
Initial pH value	7.4	7.4

We conducted *electrochemical tests* on the three Mg-based alloys mentioned above using a PARSTAT 4000 Potentiostat/Galvanostat equipment from Princeton Applied Research, USA. The measurements were made at 37 ± 0.5 °C and a pH value, for both media, of 7.4. To perform the tests, we used a typical three-electrode cell with a platinum electrode as the counter electrode (CE), the sample as the working electrode (WE), and a saturated calomel as the reference electrode (RE). The exposed area of all samples was about 1 cm^2. Before the polarization resistance experiments, we monitored the open circuit potential for 1 h. All measurements were conducted according to the ASTM G5-94 (2011) standard, ensuring accuracy and reliability. To determine the Tafel plots and to extrapolate the corrosion potential (E_{corr}) and corrosion current density (i_{corr}), we applied a potential range of ±250 mV vs. EOC (potential rich at quasi-equilibrium) at a speed of 1 mV/s. The corrosion rate was computed as presented in ASTM G102-89 [52]:

$$CR = K_i \frac{i_{corr}}{\rho} EW \quad (1)$$

where: CR represents the corrosion rate (mm/an), i_{corr} is the corrosion current density ($\mu A/cm^2$), EW represents the equivalent weight (g), ρ is the material density (g/cm^3), and $K_i = 3.27 \times 10^{-3}$ (C^{-1}).

Using the same standard, the polarization resistance R_p ($k\Omega cm^2$) was determined as follows:

$$R_p = \frac{1}{2.3} \frac{\beta_a \beta c}{\beta_a + \beta c} \frac{1}{i_{corr}} \quad (2)$$

where: β_c (mV) is the slope of the cathodic curve, and β_a (mV) is the slope of the anodic curve.

Immersion test. The mass loss determination was achieved by immersing the experimental samples in the SBF and DMEM solutions for 3, 10, and 12 days. The test media were changed daily, and a thermostatic bath (Immersion Bath Circulator LabTech Model LCB-11D) was used to maintain the samples at 37 ± 1 °C. The samples were initially weighed (before immersion in SBF and DMEM) and after removing them from the media

and removing the corrosion products using a chromic acid solution without attacking the residual magnesium alloy matrix. To ensure the accuracy of the experiment, three samples were employed for each type of Mg-based alloy. The mass loss and corrosion rate were calculated based on the following equations:

$$ML = \frac{m_0 - m_f}{m_0} \times 100 \quad (3)$$

where: ML represents the mass loss (%), m_0 is the initial mass value and m_f is the final mass value.

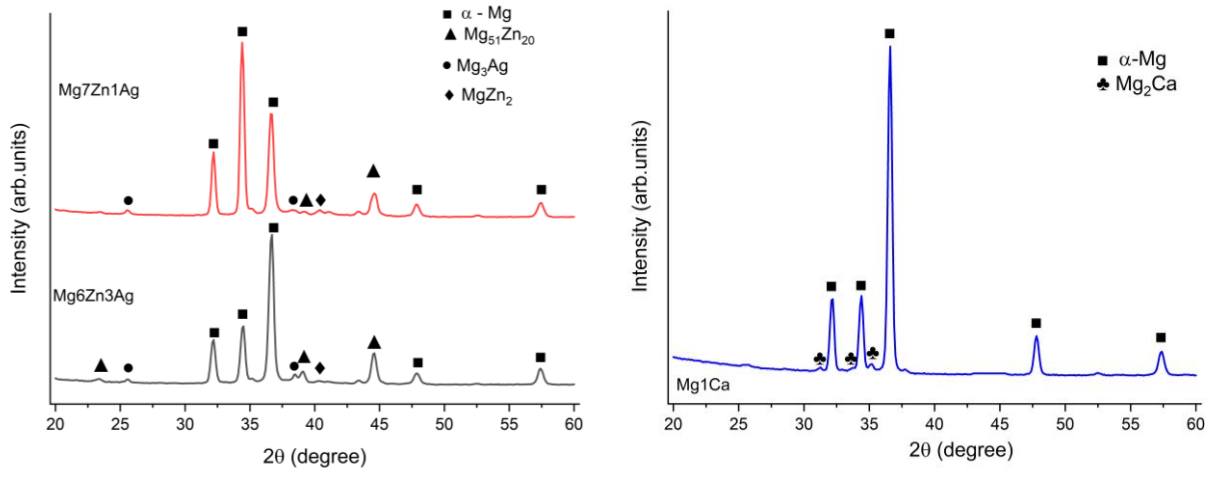
$$CR = \frac{K \times ML}{A \times t \times \rho} \quad (4)$$

where: CR represents the corrosion rate (mm/year), ML is the mass loss (g), K is a constant (8.76×10^4), A is the exposed surface area (cm^2), t is the time of exposure (h), and ρ is the material density (g/cm^3).

3. Results and Discussion

3.1. Materials Characterization

The structure of the investigated Mg-based alloys was carried out by identifying and indexing the diffraction peaks from obtained X-ray diffractograms. The XRD diffraction pattern for the Mg7Zn1Ag, Mg6Zn3Ag, and Mg1Ca investigated alloys are shown in Figure 1.



(**a**) (**b**)

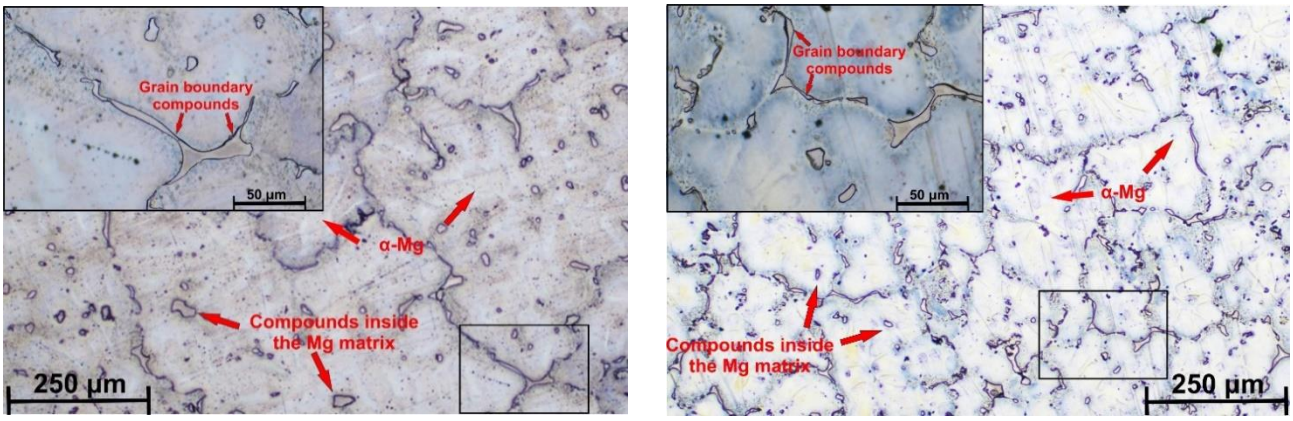
Figure 1. X-ray diffraction patterns for (**a**) Mg7Zn1Ag and Mg6Zn3Ag; (**b**) Mg1Ca investigated alloys.

As presented in Figure 1a, for the Mg-Zn-Ag ternary system alloys, there are five peaks corresponding to a major hexagonal α-Mg phase (ICDD: 04-004-8745), (100) at 2θ = 32.20°, (002) at 2θ = 34.40°, (101) at 2θ = 36.70°, (102) at 2θ = 47.92°, and (110) at 2θ = 57.40°, as well as peaks corresponding to the $MgZn_2$, $Mg_{51}Zn_{20}$, and Mg_3Ag compounds of lower intensities. By increasing the Ag content from 1 wt.% to 3 wt.%, a decrease in the peak intensity of the $MgZn_2$ compound is observed, while for the Mg_3Ag and $Mg_{51}Zn_{20}$ compounds, higher peaks are highlighted. The XRD diffractogram of Mg1Ca alloy (Figure 1b) indicates the peaks corresponding to a major hexagonal α-Mg phase and a minor hexagonal Mg_2Ca compound. The Mg_2Ca phase (ICDD: 00-013-0450) was detected at 2θ = 31.21°, 33.80°, and 35.20°, corresponding to the (103), (112), and (004) crystallographic planes. More, the α-Mg phase is observed to be present at the same 2θ

values with the same corresponding crystallographic planes as in the Mg-Zn-Ag ternary system alloys.

The addition of silver in the biodegradable magnesium alloys used for orthopaedic implants brings a series of advantages due to the modification of their microstructure. The decrease in grain size and the formation of Ag-containing secondary phases influence the mechanical properties and corrosion behaviour, which represent important factors for the success of a bone reconstruction process [46,53,54]. Razzaghi et al. [47] demonstrated that an addition between 0–3 wt.% Ag in the Mg3Zn alloy improves the hardness due to the formation of secondary phases inside and at the grain boundary. Also, Ma et al. [55] show that by increasing the Ag addition in Mg-Zn-Ca alloys from 2 wt.% to 4 wt.%, the ultimate tensile strength (UTS) increases from 235 MPa to 267 MPa, also due to the change in the alloy microstructure.

The *microstructural characteristics* of the investigated alloys were evaluated using optical microscopy and scanning electron microscopy coupled with EDS spectrometry. The obtained optical microscope images, made on the investigated as-polished Mg-based alloy samples without any chemical attack, are presented in Figures 2 and 3.



(**a**) (**b**)

Figure 2. Optical microstructure images obtained for (**a**) Mg7Zn1Ag alloy; (**b**) Mg6Zn3Ag alloy.

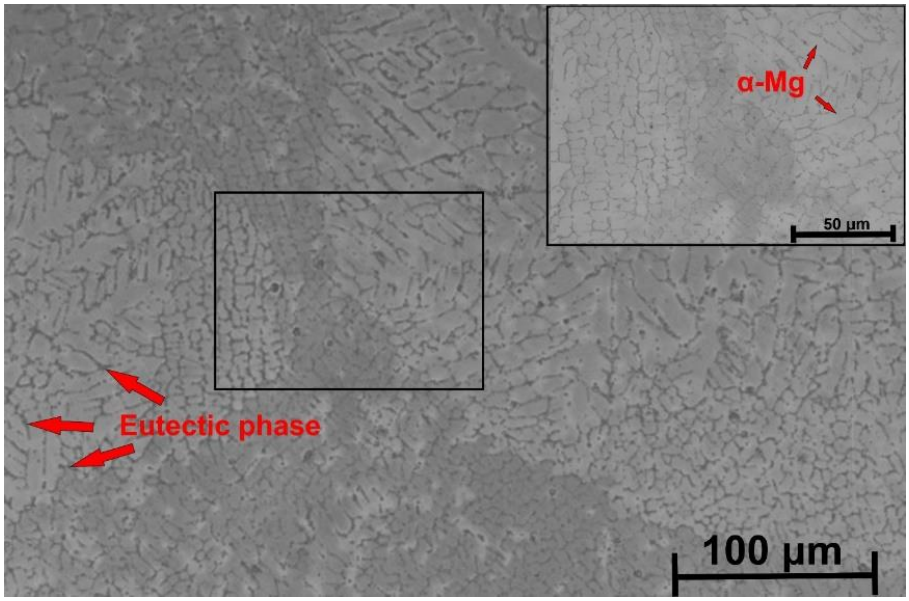


Figure 3. Optical microstructure images of the Mg1Ca alloy.

The Mg7Zn1Ag alloy microstructure highlights a coarse structure specific to a casting process, with α-Mg polyhedral grains inside, in which globular compounds can be observed. At the grain boundaries, the presence of some globular and lenticular precipitates with a morphology similar to those inside the grains is highlighted (Figure 2a). In the case of Mg6Zn3Ag alloy, smaller grains and increased precipitate density inside the magnesium matrix and grain boundary are observed (Figure 2b). So, increasing the Ag content from 1.5 wt.% to 2.5 wt.% causes grain refinement and a more pronounced grain boundary due to the accumulation of Zn and Ag precipitates in this area.

The optical microscopy images of the Mg1Ca alloy (Figure 3) indicate a biphasic structure with a dendritic aspect. The structure consists of relatively uniform α-Mg polyhedral grains (majority phase) and a distinct phase placed at the grain boundary, a eutectic (α-Mg + Mg_2Ca). The Mg_2Ca phase was formed as a lamellar structure during the alloy solidification through a eutectic reaction interrupting the magnesium matrix.

Figures 4 and 5 show the SEM micrographs of the investigated alloys. The grain boundaries and intermetallic compounds can be seen clearly.

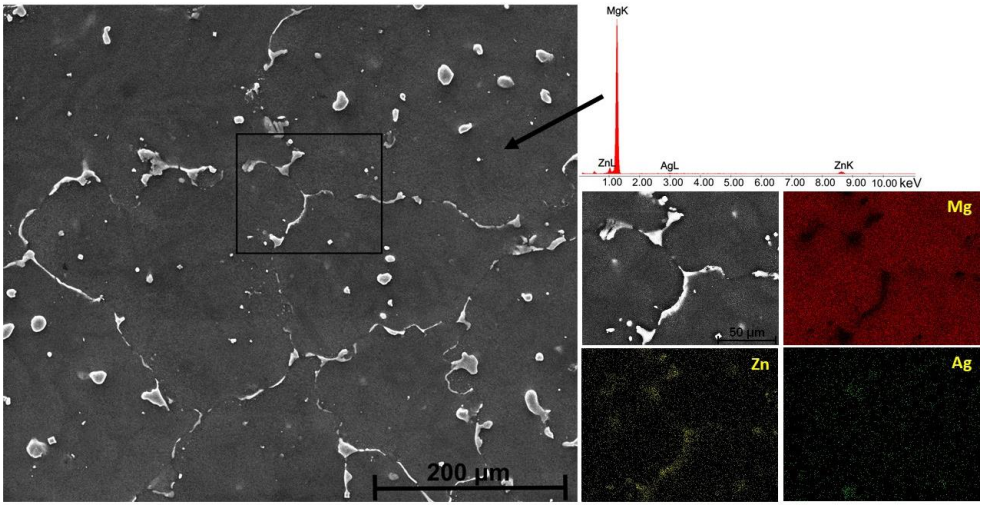


Figure 4. SEM image and corresponding EDS results for Mg7Zn1Ag alloy.

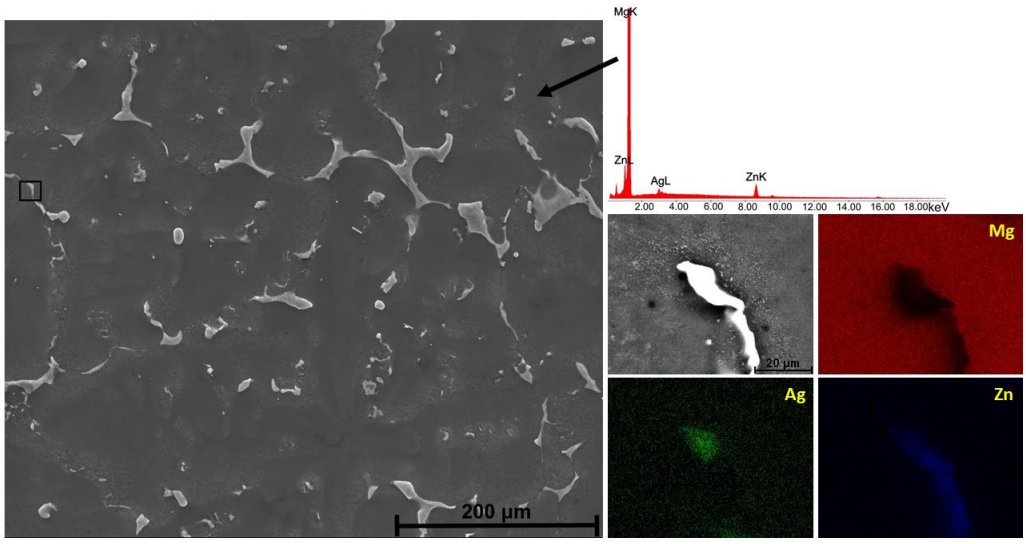


Figure 5. SEM image and corresponding EDS results for Mg6Zn3Ag alloy.

The SEM images of the Mg7Zn1Ag alloy (Figure 4) highlight the morphology and the distribution of the secondary phases ($MgZn_2$, $Mg_{51}Zn_{20}$, and Mg_3Ag). The EDS images reveal that Mg_3Ag is mainly distributed in the granular compounds in the grains and grain

boundaries. Also, the presence of Mg and Zn compounds is observed at the grain boundary in both granular and lenticular compounds ($MgZn_2$, $Mg_{51}Zn_{20}$). The Mg6Zn3Ag alloy (Figure 5) shows a morphology similar to the Mg7Zn1Ag alloy but with a high density of grain boundaries. The additional silver content was distributed both at the grain boundary (Mg_3Ag), thus preventing the grain's growth and also inside the grains. It can be said that the Ag solubility in the magnesium matrix is increased, as it is detected in a higher proportion inside the grains.

As can be seen in Figure 6, for the Mg1Ca alloy, the optical microscopy results are confirmed through the presence of the α-Mg phase (the grey area) and secondary phase with a lamellar appearance continuously distributed at the grain boundaries. According to the EDS results, the eutectic at the grain boundary consists of Mg and Ca, which confirms the existence of the Mg_2Ca phase. Also, EDS mapping images confirm that the matrix is almost entirely magnesium, and calcium is abundant along grain boundaries and on the intermetallic particles.

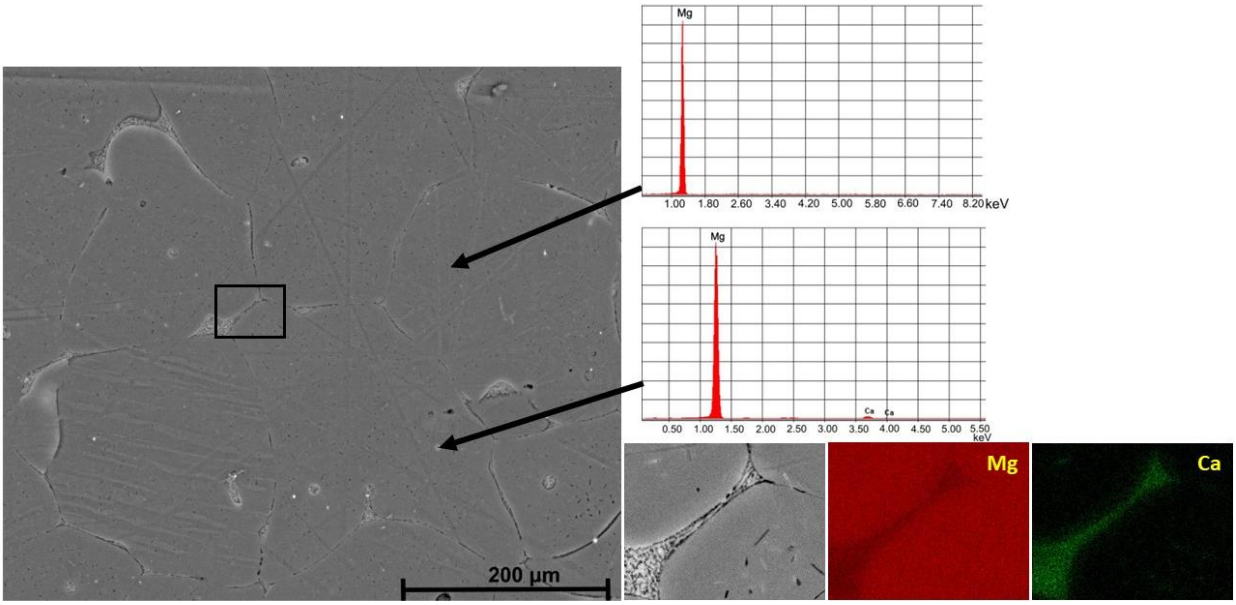


Figure 6. SEM image and corresponding EDS results for Mg1Ca alloy.

3.2. In Vitro Corrosion Study

The corrosion of magnesium and magnesium alloys in aqueous environments is mainly localized and in the form of irregular pitting, leading to magnesium hydroxide and hydrogen gas formation. According to the Pourbaix chart, magnesium hydroxide formed at the magnesium and magnesium alloy surface acts as a protective layer only in alkaline environments with pH values higher than 10.5. Also, when the chloride ion concentration is higher than 30 mmol/L, magnesium hydroxide turns into soluble magnesium chloride, leading to severe pitting corrosion [56,57]. The corrosion behaviour of the Mg-Zn-Ag ternary system alloys depends on the distribution of the Ag-containing secondary phase, the grain size, and the presence of silver as a solute element in the magnesium matrix [46,58]. The Ag-containing secondary phase (Mg_3Ag, with a corrosion potential of −2.45 V) acts as a cathode and increases the corrosion process. At the same time, the presence of Ag in the magnesium matrix improves the alloy standard electrode potential and thus enhances the corrosion behaviour.

During the corrosion of the Mg1Ca alloy in aqueous environments, the Mg_2Ca secondary phase behaves as an efficient cathode for hydrogen release due to the more Mg_2Ca positive potential to that of the α-Mg matrix. Thus, an anodic dissolution of magnesium takes place.

3.2.1. Electrochemical Tests

The Tafel curves are shown in Figure 7.

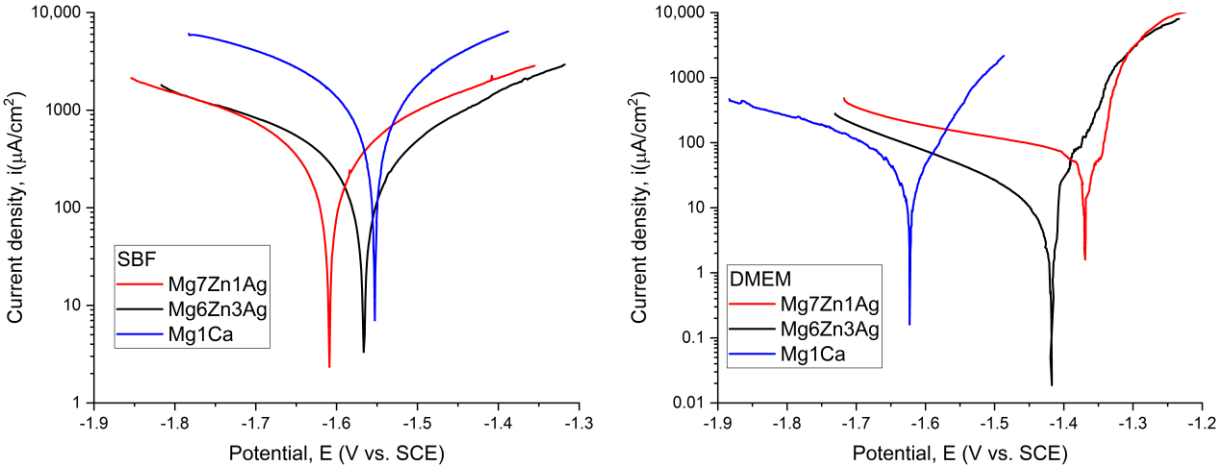


Figure 7. Tafel plots of the investigated Mg-based alloys: (**a**) in SBF; (**b**) in DMEM.

Based on the electrochemical measurements, it was observed that all samples displayed negative values below −1 V for both open circuit and corrosion potentials when SBF and DMEM media were used as an electrolyte. Generally, materials with high electropositive values for open circuit (E_{oc}) and corrosion (E_{corr}) potentials, electronegative values of corrosion current density (i_{corr}), a higher polarization (R_p) value, and a low corrosion rate (CR) are known to have good corrosion resistance [59]. The obtained results are presented in Tables 5 and 6.

Table 5. Main electrochemical parameters in SBF.

Sample	E_{oc} (V)	E_{corr} (V)	i_{corr} (μA/cm²)	CR (mm/Year)	β_c (mV)	β_a (mV)	R_p (kΩcm²)
Mg6Zn3Ag	−1.569	−1.566	990.876	22.014	901.242	517.542	0.144
Mg7Zn1Ag	−1.606	−1.609	1345.000	28.834	902.334	619.550	0.118
Mg1Ca	−1.597	−1.562	4280.000	31.247	938.810	477.510	0.032

Table 6. Main electrochemical parameters in DMEM.

Sample	E_{oc} (V)	E_{corr} (V)	i_{corr} (μA/cm²)	CR (mm/Year)	β_c (mV)	β_a (mV)	R_p (kΩcm²)
Mg6Zn3Ag	−1.455	−1.386	8.081	0.173	207.900	115.857	3.573
Mg7Zn1Ag	−1.476	−1.401	9.053	0.201	252.470	51.531	2.302
Mg0.9Ca	−1.489	−1.421	50.831	1.170	280.353	165.834	0.887

It is well known that the Zn content increases the corrosion resistance at a value lower than 5 wt.% [60,61]. Also, the literature showed that the increase in corrosion resistance due to Zn percent could be explained by the grain size refinement, better passivity of the surface, and a reduced number of impurities [61]. Zn content of over 5% wt. determines the prevalence of the $MgZn_2$ phase that rapidly increases in the matrix to generate a continuous network structure, which can be directly linked to the formation of many sites with anode–cathode behaviour. In [60], it was shown that 7 wt.% Zn has an increased corrosion effect that is mainly due to galvanic couple and has, as a result, the dissolution of α-Mg matrix. It can be noticed that when the Zn amount is lower than 5 wt.%, an increase in the Zn

percent leads to an improvement of the corrosion effect due to the grain refinement and formation of a protective surface film based on Zn [62,63]. In the case of our investigated alloys, Mg6Zn3Ag has a percent of Zn of about 6.3%wt. and Mg7Zn1Ag of 7.1 wt.%. It can be concluded that a high level of Zn will determine the apparition of the secondary phase, and they can affect the localized corrosion behaviour between them and the main matrix of the alloy. Similar observations were found by Koç et al. [64] and Yan et al. [65]. Regarding the corrosion density current and corrosion rate criteria in both physiological media, the alloys can be ranked as Mg6Zn3Ag, Mg7Zn1Ag, and Mg1Ca.

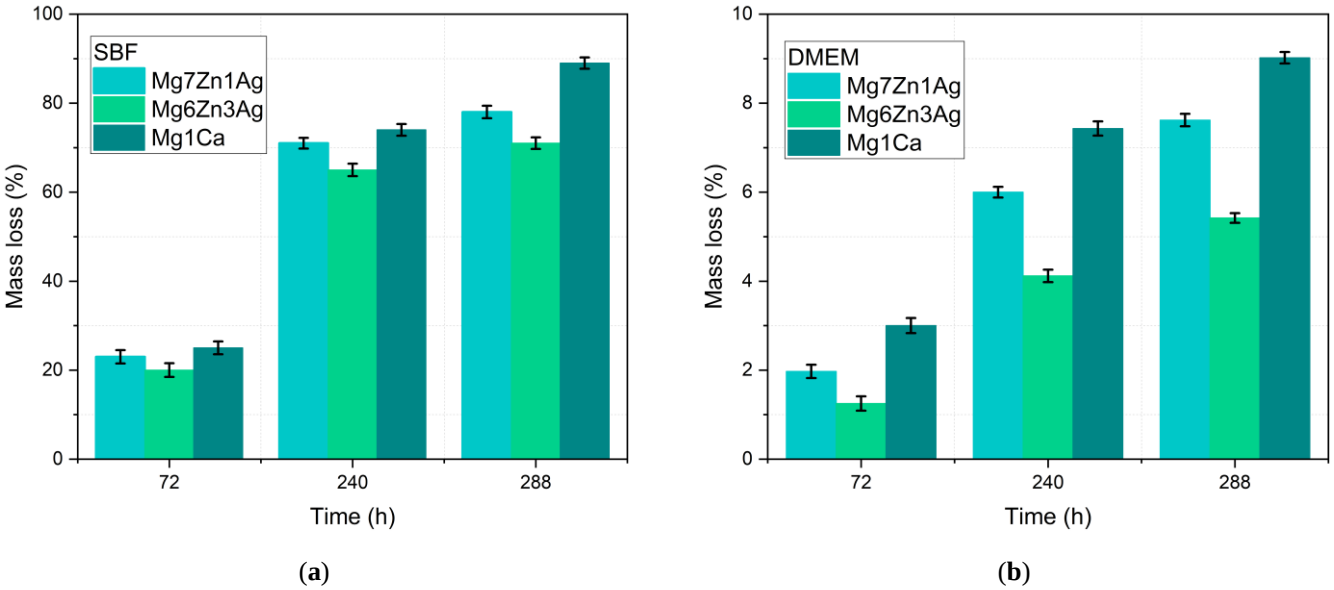
The alloys Mg6Zn3Ag and Mg7Zn1Ag are the only materials that contain silver (2.5 wt.% and 1.5 wt.%, respectively). It was observed that when the Ag percent increases, the phases Mg_3Ag and $Mg_{51}Zn_{20}$ are more pronounced, and the phase $MgZn_2$ reduces significantly [66]. The silver content strongly influences the alloy microstructure by refining the grain size and increasing the corrosion resistance. In the case of an Ag content higher than 3%, the mechanical properties and corrosion resistance are diminished due to cracks apparition. In our case, the Mg6Zn3Ag alloy with a higher percentage of silver (2.5 wt.%) exhibited a better corrosion resistance (SBF–Rp = 0.144 kΩcm^2, CR = 22.014 mm/year, and DMEM–Rp = 3.573 kΩcm^2, CR = 0.173 mm/year) than Mg-7Zn-1Ag (SBF–Rp = 0.118 kΩcm^2, CR = 28.834 mm/year, and DMEM–Rp = 2.302 kΩcm^2, CR = 0.201 mm/year). The high Ag content induces the apparition of a uniformly distributed second phase (Mg_3Ag), which determines a more refined grain structure.

The Mg-Ca alloy is known to reduce the corrosion effect when added in amounts of a few tenths of weight percents [67]. It can be observed that this alloy exhibited bad corrosion behaviour in SBF (i_{corr} = 4280 μA/cm^2, Rp = 0.032 kΩcm^2, and CR = 31.247 mm/year) and DMEM (i_{corr} = 50.831 μA/cm^2, R_p = 0.887 kΩcm^2, and CR = 1.170 mm/year) media. It is well known that different simulated media determine characteristic degradation rates of Mg-based alloys with their own degradation products [68–70]. So, in the case of SBF and DMEM media, by-products such as $Mg(OH)_2$, MgO, and $MgCO_3$ were reported [71,72]. The solubility of phases depends on environmental factors such as pH, temperature, and Mg dissolution rate. Initially, the SBF medium was developed for in vitro investigation and proved to enhance the apatite-forming process on implant material and to have a chemical composition close to that of human plasma. The sulphate ion concentration of 0.5 mM in SBF, compared to 0.81 mM in DMEM, accelerated the corrosion process in the first stage of the immersion process [73]. In [17], evidence was put that phosphate-buffered SBF increased the corrosion resistance of Mg-Mn-Zn and Mg-Mn alloys. The Cl^- ion concentration has an important effect on the $Mg(OH)_2$ product due to its low solubility. In our case, the SBF medium has 147.8 mM Cl^-, and the DMEM physiological medium is characterized by 121 mM Cl^-. Since more Cl^- ions are present in the SBF solution that chemically react with $Mg(OH)_2$, an increased corrosion rate was reported in comparison to the DMEM medium (Tables 5 and 6). A simulated physiological fluid usually is comprised of inorganic components, a buffering system, and organic substances. SBF medium does not contain proteins, but it has an important amount of Mg and Ca ions that influence the degradation behaviour of Mg alloys under cell culture conditions. The buffering system plays a main role in corrosion behaviour. In the case of DMEM physiological solution, HEPES is used, and it was noticed that it reduced the calcium phosphate and carbonate formation in the degradation layer through an important influence on the nucleation process [24,74,75]. Usually, HEPES has a negative effect on the protective layer density, and it permits the progressive diffusion effect of the Cl^- ions [76]. In an SBF medium, Tris-HCl is used which accelerates the degradation rate of pure Mg due to OH^- ions consumption [26]. Also, DMEM physiological medium contains amino acids such as L-Cystine 2HCl (0.2013 mM), Glycine (0.4 mM), L-Leucine (0.8015 mM), L-Serine (0.4 mM), L-Valine (0.8034 mM), L-Threonine (0.7983 mM), and L-Glutamine (4.0 mM) [74] that have an inhibitory effect on the corrosion phenomenon [77–79]. The influence of saccharides, such as glucosamine and galactose, was not investigated, and only glucose was considered. It was concluded that in physiological media, an increased glucose concentration in the

range from 1 gL^{-1} to 3 gL^{-1} slightly decreased the corrosion rate of Mg-based alloys [80]. In our case, only DMEM solution contains D-Glucose with a concentration of 5.5 mM, and it proved to exhibit a beneficial effect on corrosion behaviour. Further, the folic acid (Vitamin B9) that is present in the DMEM solution (0.0091 mM) has an inhibition effect on the corrosion of Mg-based alloys [79,81]. All these differences between the two investigated physiological media sustained our overall findings that the corrosion process is much slower in the DMEM medium than in the SBF due to the addition of organic substances and low concentration of Cl^- ions.

3.2.2. Immersion Test

The results of the corrosion tests performed by immersing the experimental samples in the SBF and DMEM media are presented in Figures 8 and 9.



(a) **(b)**

Figure 8. Mass loss evolution of the investigated Mg-based alloys in (**a**) SBF medium; (**b**) DMEM medium.

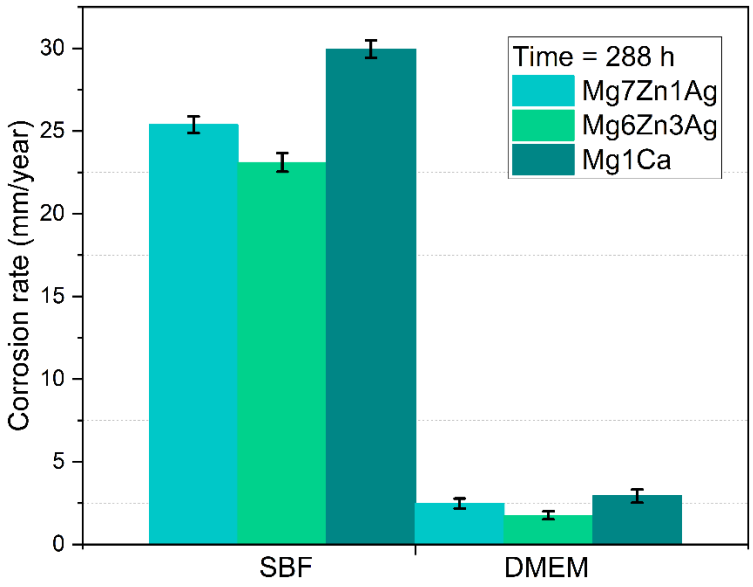


Figure 9. The corrosion rate derived from mass loss after 12 days of immersion in SBF and DMEM media.

Figure 8 highlights the mass loss of the investigated samples measured at 72, 240, and 288 h of immersion in SBF and DMEM media. The lowest mass loss was obtained for the

alloy Mg6Zn3Ag in both aqueous environments (71.09% at 288 h in SBF and 5.42% at 288 h in DMEM). The higher Ag content in the Mg6Zn3Ag alloy compared to the Mg7Zn1Ag alloy induces lower mass loss and corrosion rate (Figure 9). This behaviour is due to the grain refining as well as to the presence of silver as a dissolved element in the magnesium matrix.

We observed that the highest mass loss occurs in the first 240 h of immersion in both media, after which the variations are smaller, probably due to the increase in pH to a value at which the $Mg(OH)_2$ layer becomes stable in the immersion media.

Many studies [67,82–87] show a high corrosion rate of Mg-Ca alloys with increased Ca content. This evolution of the corrosion rate is related to more content of the Mg_2Ca intermetallic phase formed at the grain boundaries. Additionally, corrosion resistance was moderate and uniform at lower Ca content in alloys. Studies have shown that above the solid solubility limit (∼1.34 wt.% Ca), the corrosion rate increased with increasing the Ca content, and a more negative corrosion potential was observed.

The Mg1Ca alloy recorded the highest values for mass loss and corrosion rate among all investigated magnesium alloys (*ML* of 89.10% at 288 h in SBF and 9.02% at 288 h in DMEM; *CR* of 29.96 mm/year at 288 h in SBF and 2.93 mm/year at 288 h in DMEM).

Experimental results obtained for the corrosion rate and mass loss are in agreement with the results obtained from the electrochemical corrosion test in terms of both the alloy structure and the used test media. The results highlight the more corrosive nature of the SBF environment due to the presence of a larger amount of Cl^- ions, and also to the negative effect of Tris-HCl buffer on the protective layer of $Mg(OH)_2$.

4. Conclusions

The current study evaluates the influence of the microstructure and the used test media on the corrosion behaviour of the two alloys from the Mg-Zn-Ag system, respectively, Mg7Zn1Ag and Mg6Zn3Ag, and the Mg1Ca alloy. The in vitro research performed demonstrates the influence of the Mg-based alloy microstructure and the used test media on their corrosion behaviour evaluated by the corrosion rate and mass loss. The higher Ag content in the Mg6Zn3Ag alloy compared to the Mg7Zn1Ag alloy induces a lower corrosion rate and mass loss due to the grain refining as well as to the presence of silver as a dissolved element in the magnesium matrix. Also, the Ag-high content induces the apparition of a uniformly distributed second phase (Mg_3Ag), which determines a more refined grain structure.

Regarding the used test media, the experimental results highlight the more corrosive nature of the SBF environment. The Mg6Zn3Ag alloy with a higher percentage of silver (2.5 wt.%) exhibited a better corrosion resistance than Mg7Zn1Ag.

We consider that the magnesium alloy Mg6Zn3Ag showed valuable biodegradation characteristics in order to be considered as raw materials for manufacturing small trauma implants. Ultimately, future studies regarding mechanical properties and biocompatibility must confirm this assumption.

Author Contributions: Conceptualization, L.D., I.A., and M.M.; methodology, I.A., V.M., and A.A.; software, O.T. and A.S.; validation, I.A. and M.M.; formal analysis, O.T. and A.S.; investigation, L.D., A.A., A.S., M.M., C.M.C., and D.A.F.; resources, V.M., O.T., and D.A.F.; data curation, I.A., C.M.C., and V.M.; writing—original draft preparation, L.D. and A.A.; writing—review and editing, L.D. and A.A.; visualization, V.M., and D.A.F.; supervision, I.A.; project administration, L.D., and I.A.; funding acquisition, I.A. and D.A.F. All authors have read and agreed to the published version of the manuscript.

Funding: This work has been funded by the European Social Fund from the Sectoral Operational Program Human Capital 2014–2020, through the Financial Agreement with the title "Training of PhD Students and Postdoctoral Researchers in Order to Acquire Applied Research Skills—SMART", Contract No. 13530/16.06.2022—SMIS code: 153734.

Data Availability Statement: Not applicable.

Conflicts of Interest: The authors declare no conflict of interest.

References

1. Tsakiris, V.; Tardei, C.; Clicinschi, F.M. Biodegradable Mg Alloys for Orthopedic Implants–A Review. *J. Magnes. Alloys* **2021**, *9*, 1884–1905. [CrossRef]
2. Xu, T.; Yang, Y.; Peng, X.; Song, J.; Pan, F. Overview of Advancement and Development Trend on Magnesium Alloy. *J. Magnes. Alloys* **2019**, *7*, 536–544. [CrossRef]
3. Antoniac, I.; Miculescu, M.; Mănescu, V.; Stere, A.; Quan, P.H.; Păltânea, G.; Robu, A.; Earar, K. Magnesium-Based Alloys Used in Orthopedic Surgery. *Materials* **2022**, *15*, 1148. [CrossRef] [PubMed]
4. Witte, F. The History of Biodegradable Magnesium Implants: A Review☆. *Acta Biomater.* **2010**, *6*, 1680–1692. [CrossRef] [PubMed]
5. Xu, L.; Liu, X.; Sun, K.; Fu, R.; Wang, G. Corrosion Behavior in Magnesium-Based Alloys for Biomedical Applications. *Materials* **2022**, *15*, 2613. [CrossRef]
6. Elkaiam, L.; Hakimi, O.; Yosafovich-Doitch, G.; Ovadia, S.; Aghion, E. In Vivo Evaluation of Mg–5%Zn–2%Nd Alloy as an Innovative Biodegradable Implant Material. *Ann. Biomed. Eng.* **2020**, *48*, 380–392. [CrossRef]
7. Hänzi, A.C.; Gerber, I.; Schinhammer, M.; Löffler, J.F.; Uggowitzer, P.J. On the in Vitro and in Vivo Degradation Performance and Biological Response of New Biodegradable Mg–Y–Zn Alloys☆. *Acta Biomater.* **2010**, *6*, 1824–1833. [CrossRef]
8. Kraus, T.; Fischerauer, S.F.; Hänzi, A.C.; Uggowitzer, P.J.; Löffler, J.F.; Weinberg, A.M. Magnesium Alloys for Temporary Implants in Osteosynthesis: In Vivo Studies of Their Degradation and Interaction with Bone. *Acta Biomater.* **2012**, *8*, 1230–1238. [CrossRef]
9. Noviana, D.; Paramitha, D.; Ulum, M.F.; Hermawan, H. The Effect of Hydrogen Gas Evolution of Magnesium Implant on the Postimplantation Mortality of Rats. *J. Orthop. Transl.* **2016**, *5*, 9–15. [CrossRef]
10. Kim, Y.-K.; Lee, K.-B.; Kim, S.-Y.; Bode, K.; Jang, Y.-S.; Kwon, T.-Y.; Jeon, M.H.; Lee, M.-H. Gas Formation and Biological Effects of Biodegradable Magnesium in a Preclinical and Clinical Observation. *Sci. Technol. Adv. Mater.* **2018**, *19*, 324–335. [CrossRef]
11. Rahim, M.I.; Szafrański, S.P.; Ingendoh-Tsakmakidis, A.; Stiesch, M.; Mueller, P.P. Evidence for Inoculum Size and Gas Interfaces as Critical Factors in Bacterial Biofilm Formation on Magnesium Implants in an Animal Model. *Colloids Surf. B Biointerfaces* **2020**, *186*, 110684. [CrossRef] [PubMed]
12. Zhang, J.; Tang, L.; Qi, H.; Zhao, Q.; Liu, Y.; Zhang, Y. Dual Function of Magnesium in Bone Biomineralization. *Adv. Heal. Mater.* **2019**, *8*, 1901030. [CrossRef] [PubMed]
13. Zhang, X.; Dai, J.; Dong, Q.; Ba, Z.; Wu, Y. Corrosion Behavior and Mechanical Degradation of As-extruded Mg–Gd–Zn–Zr Alloys for Orthopedic Application. *J. Biomed. Mater. Res. B Appl. Biomater.* **2020**, *108*, 698–708. [CrossRef] [PubMed]
14. Miao, H.; Zhang, D.; Chen, C.; Zhang, L.; Pei, J.; Su, Y.; Huang, H.; Wang, Z.; Kang, B.; Ding, W.; et al. Research on Biodegradable Mg–Zn–Gd Alloys for Potential Orthopedic Implants: In Vitro and in Vivo Evaluations. *ACS Biomater. Sci. Eng.* **2019**, *5*, 1623–1634. [CrossRef] [PubMed]
15. Lamaka, S.V.; Gonzalez, J.; Mei, D.; Feyerabend, F.; Willumeit-Römer, R.; Zheludkevich, M.L. Local PH and Its Evolution Near Mg Alloy Surfaces Exposed to Simulated Body Fluids. *Adv. Mater. Interfaces* **2018**, *5*, 1800169. [CrossRef]
16. Zhao, Y.; Wu, G.; Jiang, J.; Wong, H.M.; Yeung, K.W.K.; Chu, P.K. Improved Corrosion Resistance and Cytocompatibility of Magnesium Alloy by Two-Stage Cooling in Thermal Treatment. *Corros. Sci.* **2012**, *59*, 360–365. [CrossRef]
17. Xu, L.; Zhang, E.; Yin, D.; Zeng, S.; Yang, K. In Vitro Corrosion Behaviour of Mg Alloys in a Phosphate Buffered Solution for Bone Implant Application. *J. Mater. Sci. Mater. Med.* **2008**, *19*, 1017–1025. [CrossRef]
18. Staiger, M.P.; Pietak, A.M.; Huadmai, J.; Dias, G. Magnesium and Its Alloys as Orthopedic Biomaterials: A Review. *Biomaterials* **2006**, *27*, 1728–1734. [CrossRef]
19. Witte, F.; Kaese, V.; Haferkamp, H.; Switzer, E.; Meyer-Lindenberg, A.; Wirth, C.J.; Windhagen, H. In Vivo Corrosion of Four Magnesium Alloys and the Associated Bone Response. *Biomaterials* **2005**, *26*, 3557–3563. [CrossRef]
20. Ran, Z.; Dai, W.; Xie, K.; Hao, Y. Advances of Biodegradable Magnesium-Based Implants for Orthopaedics. *Life Res.* **2022**, *5*, 7. [CrossRef]
21. Xin, Y.; Hu, T.; Chu, P.K. In Vitro Studies of Biomedical Magnesium Alloys in a Simulated Physiological Environment: A Review. *Acta Biomater.* **2011**, *7*, 1452–1459. [CrossRef] [PubMed]
22. Gu, X.N.; Zheng, W.; Cheng, Y.; Zheng, Y.F. A Study on Alkaline Heat Treated Mg–Ca Alloy for the Control of the Biocorrosion Rate. *Acta Biomater.* **2009**, *5*, 2790–2799. [CrossRef] [PubMed]
23. Gonzalez, J.; Hou, R.Q.; Nidadavolu, E.P.S.; Willumeit-Römer, R.; Feyerabend, F. Magnesium Degradation under Physiological Conditions–Best Practice. *Bioact. Mater.* **2018**, *3*, 174–185. [CrossRef] [PubMed]
24. Naddaf Dezfuli, S.; Huan, Z.; Mol, J.M.C.; Leeflang, M.A.; Chang, J.; Zhou, J. Influence of HEPES Buffer on the Local PH and Formation of Surface Layer during in Vitro Degradation Tests of Magnesium in DMEM. *Prog. Nat. Sci. Mater. Int.* **2014**, *24*, 531–538. [CrossRef]
25. Zainal Abidin, N.I.; Rolfe, B.; Owen, H.; Malisano, J.; Martin, D.; Hofstetter, J.; Uggowitzer, P.J.; Atrens, A. The in Vivo and in Vitro Corrosion of High-Purity Magnesium and Magnesium Alloys WZ21 and AZ91. *Corros. Sci.* **2013**, *75*, 354–366. [CrossRef]
26. Xin, Y.; Hu, T.; Chu, P.K. Influence of Test Solutions on In Vitro Studies of Biomedical Magnesium Alloys. *J. Electrochem. Soc.* **2010**, *157*, C238. [CrossRef]
27. Ellison, G.; Straumfjord, J.V.; Hummel, J.P. Buffer Capacities of Human Blood and Plasma. *Clin. Chem.* **1958**, *4*, 452–461. [CrossRef]
28. Lorenz, C.; Brunner, J.G.; Kollmannsberger, P.; Jaafar, L.; Fabry, B.; Virtanen, S. Effect of Surface Pre-Treatments on Biocompatibility of Magnesium. *Acta Biomater.* **2009**, *5*, 2783–2789. [CrossRef]

29. Galvin, E.; Jaiswal, S.; Lally, C.; MacDonald, B.; Duffy, B. In Vitro Corrosion and Biological Assessment of Bioabsorbable WE43 Mg Alloy Specimens. *J. Manuf. Mater. Process.* **2017**, *1*, 8. [CrossRef]
30. Walker, J.; Shadanbaz, S.; Woodfield, T.B.F.; Staiger, M.P.; Dias, G.J. The in Vitro and in Vivo Evaluation of the Biocompatibility of Mg Alloys. *Biomed. Mater.* **2013**, *9*, 015006. [CrossRef]
31. Wang, J.; Giridharan, V.; Shanov, V.; Xu, Z.; Collins, B.; White, L.; Jang, Y.; Sankar, J.; Huang, N.; Yun, Y. Flow-Induced Corrosion Behavior of Absorbable Magnesium-Based Stents. *Acta Biomater.* **2014**, *10*, 5213–5223. [CrossRef] [PubMed]
32. Marco, I.; Feyerabend, F.; Willumeit-Römer, R.; Van der Biest, O. Degradation Testing of Mg Alloys in Dulbecco's Modified Eagle Medium: Influence of Medium Sterilization. *Mater. Sci. Eng. C* **2016**, *62*, 68–78. [CrossRef] [PubMed]
33. Bowen, P.K.; Drelich, J.; Goldman, J. A New in Vitro–in Vivo Correlation for Bioabsorbable Magnesium Stents from Mechanical Behavior. *Mater. Sci. Eng. C* **2013**, *33*, 5064–5070. [CrossRef]
34. Gutiérrez Púa, L.D.C.; Rincón Montenegro, J.C.; Fonseca Reyes, A.M.; Zambrano Rodríguez, H.; Paredes Méndez, V.N. Biomaterials for Orthopedic Applications and Techniques to Improve Corrosion Resistance and Mechanical Properties for Magnesium Alloy: A Review. *J. Mater. Sci.* **2023**, *58*, 3879–3908. [CrossRef]
35. Tong, X.; Zhang, D.; Lin, J.; Dai, Y.; Luan, Y.; Sun, Q.; Shi, Z.; Wang, K.; Gao, Y.; Lin, J.; et al. Development of Biodegradable Zn–1Mg–0.1RE (RE = Er, Dy, and Ho) Alloys for Biomedical Applications. *Acta Biomater.* **2020**, *117*, 384–399. [CrossRef]
36. Mohamed, A.; El-Aziz, A.M.; Breitinger, H.-G. Study of the Degradation Behavior and the Biocompatibility of Mg–0.8Ca Alloy for Orthopedic Implant Applications. *J. Magnes. Alloys* **2019**, *7*, 249–257. [CrossRef]
37. Makkar, P.; Sarkar, S.K.; Padalhin, A.R.; Moon, B.-G.; Lee, Y.S.; Lee, B.T. In Vitro and in Vivo Assessment of Biomedical Mg–Ca Alloys for Bone Implant Applications. *J. Appl. Biomater. Funct. Mater.* **2018**, *16*, 126–136. [CrossRef]
38. Lee, S.; Lee, D.; Lee, K.; Park, C.; Lim, H.; Park, S.; Kyungku, L.; Yun, K. Evaluation of Bioabsorbable Mg–Mn Alloy with Anodic Oxidation Treatment. *J. Nanosci. Nanotechnol.* **2020**, *20*, 5625–5628. [CrossRef] [PubMed]
39. Hu, Y.; Guo, X.; Qiao, Y.; Wang, X.; Lin, Q. Preparation of Medical Mg–Zn Alloys and the Effect of Different Zinc Contents on the Alloy. *J. Mater. Sci. Mater. Med.* **2022**, *33*, 9. [CrossRef]
40. Martin, A.; Vilanova, M.; Gil, E.; Sebastian, M.S.; Wang, C.Y.; Milenkovic, S.; Pérez-Prado, M.T.; Cepeda-Jiménez, C.M. Influence of the Zr Content on the Processability of a High Strength Al-Zn-Mg-Cu-Zr Alloy by Laser Powder Bed Fusion. *Mater. Charact.* **2022**, *183*, 111650. [CrossRef]
41. Wang, G.; Song, D.; Li, C.; Klu, E.E.; Qiao, Y.; Sun, J.; Jiang, J.; Ma, A. Developing Improved Mechanical Property and Corrosion Resistance of Mg-9Li Alloy via Solid-Solution Treatment. *Metals* **2019**, *9*, 920. [CrossRef]
42. Dong, J.; Tan, L.; Yang, J.; Wang, Y.; Chen, J.; Wang, W.; Zhao, D.; Yang, K. In Vitro and in Vivo Studies on Degradation and Bone Response of Mg-Sr Alloy for Treatment of Bone Defect. *Mater. Technol.* **2018**, *33*, 387–397. [CrossRef]
43. Grimm, M.; Lohmüller, A.; Singer, R.F.; Virtanen, S. Influence of the Microstructure on the Corrosion Behaviour of Cast Mg-Al Alloys. *Corros. Sci.* **2019**, *155*, 195–208. [CrossRef]
44. Zeng, R.; Dietzel, W.; Witte, F.; Hort, N.; Blawert, C. Progress and Challenge for Magnesium Alloys as Biomaterials. *Adv. Eng. Mater.* **2008**, *10*, B3–B14. [CrossRef]
45. Thomann, M.; Krause, C.; Angrisani, N.; Bormann, D.; Hassel, T.; Windhagen, H.; Meyer-Lindenberg, A. Influence of a Magnesium-Fluoride Coating of Magnesium-Based Implants (MgCa0.8) on Degradation in a Rabbit Model. *J. Biomed. Mater. Res. A* **2010**, *93*, 1609–1619. [CrossRef]
46. Mohammadi Zerankeshi, M.; Alizadeh, R. Ag-Incorporated Biodegradable Mg Alloys. *Materialia* **2022**, *23*, 101445. [CrossRef]
47. Razzaghi, M.; Kasiri-Asgarani, M.; Bakhsheshi-Rad, H.R.; Ghayour, H. In Vitro Degradation, Antibacterial Activity and Cytotoxicity of Mg-3Zn-XAg Nanocomposites Synthesized by Mechanical Alloying for Implant Applications. *J. Mater. Eng. Perform.* **2019**, *28*, 1441–1455. [CrossRef]
48. Rau, J.V.; Antoniac, I.; Fosca, M.; De Bonis, A.; Blajan, A.I.; Cotrut, C.; Graziani, V.; Curcio, M.; Cricenti, A.; Niculescu, M.; et al. Glass-Ceramic Coated Mg-Ca Alloys for Biomedical Implant Applications. *Mater. Sci. Eng. C* **2016**, *64*, 362–369. [CrossRef]
49. Bita, A.-I.; Stan, G.E.; Niculescu, M.; Ciuca, I.; Vasile, E.; Antoniac, I. Adhesion Evaluation of Different Bioceramic Coatings on Mg–Ca Alloys for Biomedical Applications. *J. Adhes. Sci. Technol.* **2016**, *30*, 1968–1983. [CrossRef]
50. Bita, A.I.; Semenescu, A.; Antoniac, A.; Antoniac, I. Hydrogen Evolution Analyzed on Various Magnesium Alloys. *Key Eng. Mater.* **2016**, *695*, 152–156. [CrossRef]
51. Kokubo, T.; Takadama, H. How Useful Is SBF in Predicting in Vivo Bone Bioactivity? *Biomaterials* **2006**, *27*, 2907–2915. [CrossRef] [PubMed]
52. *ASTM Standard G102-89*; Standard Practice for Calculation of Corrosion Rates and Related Information from Electrochemical Measurements. Annual Book of ASTM Standards; ASTM International: West Conshohocken, PA, USA, 2006; Volume 3, pp. 1–7. Available online: https://www.astm.org/g0102-89r15e01.html (accessed on 11 May 2023).
53. Son, H.-T.; Kim, D.-G.; Park, J.S. Effects of Ag Addition on Microstructures and Mechanical Properties of Mg–6Zn–2Sn–0.4Mn-Based Alloy System. *Mater. Lett.* **2011**, *65*, 3150–3153. [CrossRef]
54. Tie, D.; Feyerabend, F.; Hort, N.; Hoeche, D.; Kainer, K.U.; Willumeit, R.; Mueller, W.D. In Vitro Mechanical and Corrosion Properties of Biodegradable Mg-Ag Alloys. *Mater. Corros.* **2014**, *65*, 569–576. [CrossRef]
55. Ma, Y.; Wang, D.; Li, H.; Yuan, F.; Yang, C.; Zhang, J. Microstructure, Mechanical and Corrosion Properties of Novel Quaternary Biodegradable Extruded Mg–1Zn–0.2Ca-XAg Alloys. *Mater. Res. Express* **2020**, *7*, 015414. [CrossRef]

56. Witte, F.; Hort, N.; Vogt, C.; Cohen, S.; Kainer, K.U.; Willumeit, R.; Feyerabend, F. Degradable Biomaterials Based on Magnesium Corrosion. *Curr. Opin. Solid State Mater. Sci.* **2008**, *12*, 63–72. [CrossRef]
57. Neves, C.S.; Sousa, I.; Freitas, M.A.; Moreira, L.; Costa, C.; Teixeira, J.P.; Fraga, S.; Pinto, E.; Almeida, A.; Scharnagl, N.; et al. Insights into Corrosion Behaviour of Uncoated Mg Alloys for Biomedical Applications in Different Aqueous Media. *J. Mater. Res. Technol.* **2021**, *13*, 1908–1922. [CrossRef]
58. Argade, G.R.; Panigrahi, S.K.; Mishra, R.S. Effects of Grain Size on the Corrosion Resistance of Wrought Magnesium Alloys Containing Neodymium. *Corros. Sci.* **2012**, *58*, 145–151. [CrossRef]
59. Liao, B.; Ma, S.; Zhang, S.; Li, X.; Quan, R.; Wan, S.; Guo, X. Fructus cannabis protein extract powder as a green and high effective corrosion inhibitor for Q235 carbon steel in 1 M HCl solution. *Int. J. Biol. Macromol.* **2023**, *239*, 124358. [CrossRef]
60. Cai, S.; Lei, T.; Li, N.; Feng, F. Effects of Zn on Microstructure, Mechanical Properties and Corrosion Behavior of Mg–Zn Alloys. *Mater. Sci. Eng. C* **2012**, *32*, 2570–2577. [CrossRef]
61. Jiang, P.; Blawert, C.; Zheludkevich, M.L. The Corrosion Performance and Mechanical Properties of Mg-Zn Based Alloys—A Review. *Corros. Mater. Degrad.* **2020**, *1*, 7. [CrossRef]
62. Song, Y.; Han, E.H.; Shan, D.; Yim, C.D.; You, B.S. The Role of Second Phases in the Corrosion Behavior of Mg-5Zn Alloy. *Corros. Sci.* **2012**, *60*, 238–245. [CrossRef]
63. Bakhsheshi-Rad, H.R.; Hamzah, E.; Medraj, M.; Idris, M.H.; Lotfabadi, A.F.; Daroonparvar, M.; Yajid, M.A.M. Effect of Heat Treatment on the Microstructure and Corrosion Behaviour of Mg-Zn Alloys. *Mater. Corros.* **2014**, *65*, 999–1006. [CrossRef]
64. Koç, E.; Kannan, M.B.; Ünal, M.; Candan, E. Influence of Zinc on the Microstructure, Mechanical Properties and in Vitro Corrosion Behavior of Magnesium–Zinc Binary Alloys. *J. Alloys Compd.* **2015**, *648*, 291–296. [CrossRef]
65. Yan, Y.; Cao, H.; Kang, Y.; Yu, K.; Xiao, T.; Luo, J.; Deng, Y.; Fang, H.; Xiong, H.; Dai, Y. Effects of Zn Concentration and Heat Treatment on the Microstructure, Mechanical Properties and Corrosion Behavior of as-Extruded Mg-Zn Alloys Produced by Powder Metallurgy. *J. Alloys Compd.* **2017**, *693*, 1277–1289. [CrossRef]
66. Dragomir Nicolescu, L.; Antoniac, A.; Manescu Paltanea, V.; Robu, A.; Dinu, M.; Pana, I.; Cotrut, C.M.; Kamel, E.; Antoniac, I.; Rau, J.V.; et al. Preparation and Characterization of Hydroxyapatite Coating by Magnetron Sputtering on Mg–Zn–Ag Alloys for Orthopaedic Trauma Implants. *Ceram. Int.* **2023**, *49*, 26274–26288. [CrossRef]
67. Gu, X.N.; Zheng, Y.F.; Chen, L.J. Influence of Artificial Biological Fluid Composition on the Biocorrosion of Potential Orthopedic Mg–Ca, AZ31, AZ91 Alloys. *Biomed. Mater.* **2009**, *4*, 065011. [CrossRef]
68. Yang, L.; Zhang, E. Biocorrosion Behavior of Magnesium Alloy in Different Simulated Fluids for Biomedical Application. *Mater. Sci. Eng. C* **2009**, *29*, 1691–1696. [CrossRef]
69. Rettig, R.; Virtanen, S. Composition of Corrosion Layers on a Magnesium Rare-Earth Alloy in Simulated Body Fluids. *J. Biomed. Mater. Res. A* **2009**, *88A*, 359–369. [CrossRef]
70. Yamamoto, A.; Hiromoto, S. Effect of Inorganic Salts, Amino Acids and Proteins on the Degradation of Pure Magnesium in Vitro. *Mater. Sci. Eng. C* **2009**, *29*, 1559–1568. [CrossRef]
71. Tie, D.; Feyerabend, F.; Hort, N.; Willumeit, R.; Hoeche, D. XPS Studies of Magnesium Surfaces after Exposure to Dulbecco's Modified Eagle Medium, Hank's Buffered Salt Solution, and Simulated Body Fluid. *Adv. Eng. Mater.* **2010**, *12*, B699–B704. [CrossRef]
72. Esmaily, M.; Svensson, J.E.; Fajardo, S.; Birbilis, N.; Frankel, G.S.; Virtanen, S.; Arrabal, R.; Thomas, S.; Johansson, L.G. Fundamentals and Advances in Magnesium Alloy Corrosion. *Prog. Mater. Sci.* **2017**, *89*, 92–193. [CrossRef]
73. Xin, Y.; Huo, K.; Tao, H.; Tang, G.; Chu, P.K. Influence of Aggressive Ions on the Degradation Behavior of Biomedical Magnesium Alloy in Physiological Environment. *Acta Biomater.* **2008**, *4*, 2008–2015. [CrossRef]
74. Biţa, A.-I.; Antoniac, I.; Miculescu, M.; Stan, G.E.; Leonat, L.; Antoniac, A.; Constantin, B.; Forna, N. Electrochemical and In Vitro Biological Evaluation of Bio-Active Coatings Deposited by Magnetron Sputtering onto Biocompatible Mg-0.8Ca Alloy. *Materials* **2022**, *15*, 3100. [CrossRef]
75. Kirkland, N.T.; Waterman, J.; Birbilis, N.; Dias, G.; Woodfield, T.B.F.; Hartshorn, R.M.; Staiger, M.P. Buffer-Regulated Biocorrosion of Pure Magnesium. *J. Mater. Sci. Mater. Med.* **2012**, *23*, 283–291. [CrossRef]
76. Törne, K.; Örnberg, A.; Weissenrieder, J. The Influence of Buffer System and Biological Fluids on the Degradation of Magnesium. *J. Biomed. Mater. Res. B Appl. Biomater.* **2017**, *105*, 1490–1502. [CrossRef] [PubMed]
77. Helal, N.H.; Badawy, W.A. Environmentally Safe Corrosion Inhibition of Mg–Al–Zn Alloy in Chloride Free Neutral Solutions by Amino Acids. *Electrochim. Acta* **2011**, *56*, 6581–6587. [CrossRef]
78. Fang, Z.; Wang, J.; Yang, X.; Sun, Q.; Jia, Y.; Liu, H.; Xi, T.; Guan, S. Adsorption of Arginine, Glycine and Aspartic Acid on Mg and Mg-Based Alloy Surfaces: A First-Principles Study. *Appl. Surf. Sci.* **2017**, *409*, 149–155. [CrossRef]
79. Wang, Y.; Ding, B.-H.; Gao, S.-Y.; Chen, X.-B.; Zeng, R.-C.; Cui, L.-Y.; Li, S.-J.; Li, S.-Q.; Zou, Y.-H.; Han, E.-H.; et al. In Vitro Corrosion of Pure Mg in Phosphate Buffer Solution—Influences of Isoelectric Point and Molecular Structure of Amino Acids. *Mater. Sci. Eng. C* **2019**, *105*, 110042. [CrossRef] [PubMed]
80. Zeng, R.-C.; Li, X.-T.; Li, S.-Q.; Zhang, F.; Han, E.-H. In Vitro Degradation of Pure Mg in Response to Glucose. *Sci. Rep.* **2015**, *5*, 13026. [CrossRef]
81. Zhao, Y.; Qiao, C.; Fang, Z.; Wang, H.; Zhu, S.; Wang, J.; Ren, J.; Guan, S.; Jia, Y. Inverted Hydration Layers on Bio-Magnesium Surfaces in the Initial Degradation Stage and Their Influence on Adsorption of Amino Acid Analogues: The Metadynamics Simulations. *Langmuir* **2019**, *35*, 17009–17015. [CrossRef]

82. Kannan, M.B.; Raman, R.K.S. In Vitro Degradation and Mechanical Integrity of Calcium-Containing Magnesium Alloys in Modified-Simulated Body Fluid. *Biomaterials* **2008**, *29*, 2306–2314. [CrossRef]
83. Kirkland, N.T.; Birbilis, N.; Walker, J.; Woodfield, T.; Dias, G.J.; Staiger, M.P. In-Vitro Dissolution of Magnesium-Calcium Binary Alloys: Clarifying the Unique Role of Calcium Additions in Bioresorbable Magnesium Implant Alloys. *J. Biomed. Mater. Res. B Appl. Biomater.* **2010**, *95B*, 91–100. [CrossRef]
84. Rad, H.R.B.; Idris, M.H.; Kadir, M.R.A.; Farahany, S. Microstructure Analysis and Corrosion Behavior of Biodegradable Mg–Ca Implant Alloys. *Mater. Des.* **2012**, *33*, 88–97. [CrossRef]
85. Witte, F.; Fischer, J.; Maier, P.; Blawert, C.; Stormer, M.; Hort, M. Magnesium-Hydroxyapatite Composites as an Approach to Degradable Biomaterials. In Proceedings of the Magnesium. In Proceedings of the 7th International Conference on Magnesium Alloys and Their Applications, Dresden, Germany, 6–9 November 2006; Wiley, VCH: Weinheim, Germany, 2007; pp. 958–964, ISBN 3-527-31764-3.
86. Liu, C.L.; Wang, Y.J.; Zeng, R.C.; Zhang, X.M.; Huang, W.J.; Chu, P.K. In Vitro Corrosion Degradation Behaviour of Mg–Ca Alloy in the Presence of Albumin. *Corros. Sci.* **2010**, *52*, 3341–3347. [CrossRef]
87. Salahshoor, M.; Guo, Y. Biodegradable Orthopedic Magnesium-Calcium (MgCa) Alloys, Processing, and Corrosion Performance. *Materials* **2012**, *5*, 135–155. [CrossRef] [PubMed]

Disclaimer/Publisher's Note: The statements, opinions and data contained in all publications are solely those of the individual author(s) and contributor(s) and not of MDPI and/or the editor(s). MDPI and/or the editor(s) disclaim responsibility for any injury to people or property resulting from any ideas, methods, instructions or products referred to in the content.